





Toroidal density-equalizing map for genus-one surfaces

Shunyu Yao , Gary P.T. Choi *

Department of Mathematics, The Chinese University of Hong Kong, Hong Kong, China

ARTICLE INFO

Dataset link: <https://github.com/garyptchoi/toroidal-density-equalizing-map>

Keywords:

Density-equalizing map
Torus
Genus-one surfaces
Surface parameterization
Area-preserving map

ABSTRACT

Density-equalizing map is a shape deformation technique originally developed for cartogram creation and sociological data visualization on planar geographical maps. In recent years, there has been an increasing interest in developing density-equalizing mapping methods for surface and volumetric domains and applying them to various problems in geometry processing and imaging science. However, the existing surface density-equalizing mapping methods are only applicable to surfaces with relatively simple topologies but not surfaces with topological holes. In this work, we develop a novel algorithm for computing density-equalizing maps for toroidal surfaces. In particular, different shape deformation effects can be easily achieved by prescribing different population functions on the torus and performing diffusion-based deformations on a planar domain with periodic boundary conditions. Furthermore, the proposed toroidal density-equalizing mapping method naturally leads to an effective method for computing toroidal parameterizations of genus-one surfaces with controllable area changes, with the toroidal area-preserving parameterization being a prime example. Experimental results are presented to demonstrate the effectiveness of our proposed methods.

1. Introduction

The density-equalizing map is a technique proposed by Gastner and Newman [1] for cartogram creation. It produces a shape deformation on a planar domain based on the physical principle of density diffusion. Over the past few decades, the technique has been widely used for the visualization and analysis of sociological data, including global epidemics [2], species extinction [3], climate warming [4], democratization [5], and social media usage [6]. In recent years, there have been continuous efforts in the development and analysis of the density-equalizing map and its variants. For instance, Gastner et al. [7] developed a fast flow-based method for computing density-equalizing maps with improved efficiency. Several works have also studied the effectiveness of contiguous area cartograms [8,9]. Another recent direction has been the development of density-equalizing mapping methods for more general domains. In [10], Choi and Rycroft proposed a mapping method for simply connected open surfaces based on the density-equalizing map technique. Later, Lyu et al. [11] developed an extension of the density-equalizing mapping method for multiply connected open surfaces. Some other recent works have also developed density-equalizing mapping methods for genus-0 closed surfaces [12–14] and volumetric domains [15,16]. Many of the above-mentioned surface and volumetric density-equalizing mapping methods have been applied to medical imaging [17], volumetric data visualization [16] and shape analysis [18,19].

As pointed out in [10], the computation of density-equalizing maps is closely related to the problem of surface parameterization, which refers to the process of mapping a complicated surface onto a simple domain with some prescribed mapping criteria. Over the past several decades, numerous surface parameterization methods have been developed [20,21]. In particular, most prior works have only focused on simply connected open surfaces (topological disk) and genus-0 closed surfaces (topological sphere), while the surface

* Corresponding author.

E-mail addresses: syyao@link.cuhk.edu.hk (S. Yao), ptchoi@cuhk.edu.hk (G.P.T. Choi).

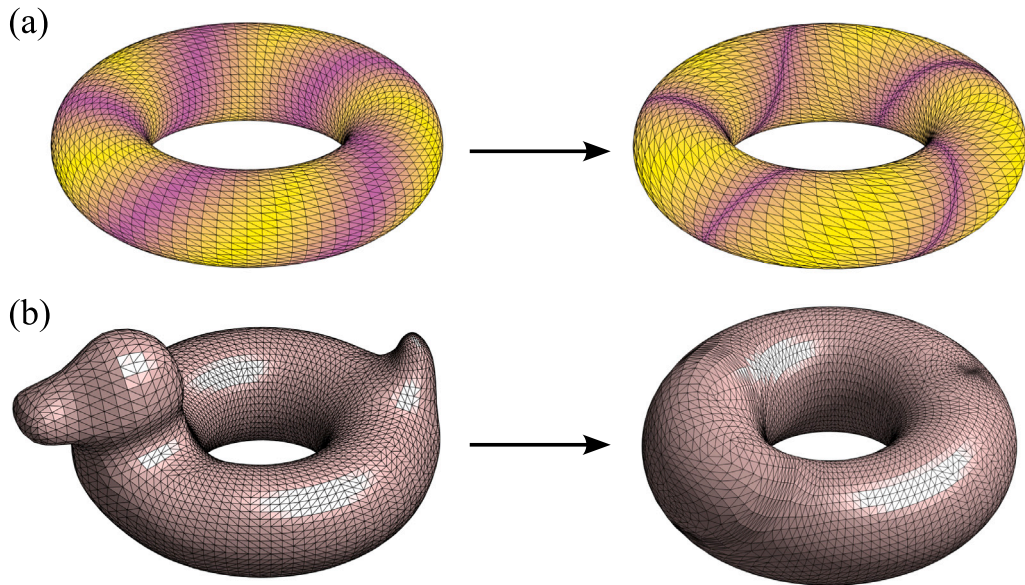


Fig. 1. An illustration of the proposed toroidal density-equalizing map and toroidal parameterization methods. (a) Using the proposed toroidal density-equalizing map (TDEM) algorithm, we can achieve shape deformations on a toroidal surface with different regions enlarged or shrunk based on some given density information. (b) Using the proposed toroidal density-equalizing parameterization method, we can effectively map a genus-one surface onto a prescribed torus with controllable area changes.

parameterization of more topologically complex surfaces is much less studied. For genus-one surfaces, Steiner and Fischer [22] developed a method for the planar parameterization of genus-one closed surfaces. Also, Ray et al. [23] developed a periodic global parameterization method that can be applied to genus-one surfaces. Zeng et al. [24] developed a method for conformally mapping a genus-one surface onto a two-layered sphere. Lam et al. [25] developed a method for landmark-constrained genus-one surface mapping using Teichmüller extremal maps. More recently, Yueh et al. [26] proposed a volume-preserving parameterization method for genus-one three-manifolds.

While density-equalizing mapping techniques have been extensively studied and used for problems involving simple topologies, their high-genus analog has not been explored. In this work, we develop a novel method for computing density-equalizing maps for toroidal surfaces (abbreviated as TDEM) based on the principle of density diffusion (Fig. 1(a)). Using the proposed method, we can create different shape deformation effects on the given toroidal surface while preserving its overall geometry by simply changing the input density. We then further develop a toroidal density-equalizing parameterization method for general genus-one surfaces based on the proposed TDEM method, which allows us to easily control the local area changes and achieve toroidal area-preserving parameterizations (Fig. 1(b)).

The organization of this paper is as follows. In Section 2, we introduce the basic concepts of density diffusion and the formulation of density-equalizing maps. In Section 3, we present our proposed TDEM method for computing toroidal density-equalizing maps. In Section 4, we describe our proposed toroidal parameterization method for general genus-one surfaces based on the proposed TDEM method. In Section 5, we present various numerical experiments to assess the performance of our proposed methods and demonstrate their effectiveness. We conclude our work and discuss possible future directions in Section 6.

2. Density diffusion and density-equalizing maps

In this section, we describe the basic principles of density diffusion and density-equalizing maps.

The density-equalizing mapping method was originally developed by Gastner and Newman [1] as a diffusion-based cartogram creation technique. Given a planar domain D representing a geographical map and a positive “population” function defined on every part of the domain, where the “population” can be human population, income, GDP, or other given data. The density-equalizing map aims to deform D to equalize the density $\rho(\mathbf{x}, t)$, which is defined as the population of position \mathbf{x} divided by its area and will be changed as time t flows. We follow the principle of density diffusion to equalize ρ and have the advection equation

$$\frac{\partial \rho}{\partial t} + \nabla \cdot \mathbf{J} = 0, \quad (1)$$

where $\mathbf{J} = \rho(\mathbf{x}, t)\mathbf{v}(\mathbf{x}, t)$ is the flux and $\mathbf{v}(\mathbf{x}, t)$ is the velocity vector. The flux \mathbf{J} can also be given by the Fick’s law:

$$\mathbf{J} = -D\nabla\rho. \quad (2)$$

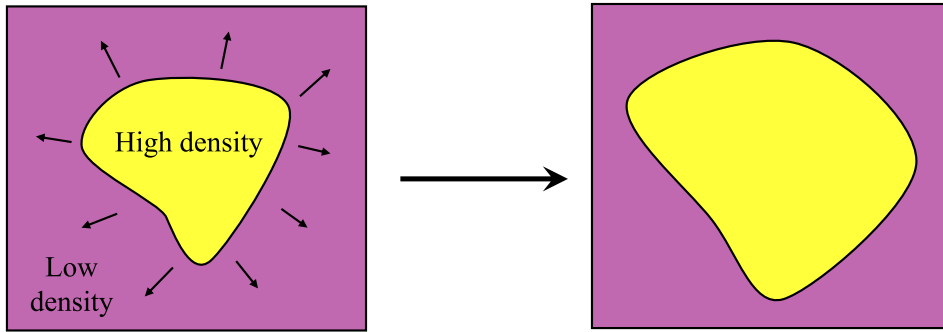


Fig. 2. An illustration of density-equalizing maps. Given a planar domain D with some high-density regions (yellow) and some low-density regions (purple), the density-equalizing map will produce a shape deformation based on the density diffusion process. In particular, the high-density regions will expand and the low-density regions will shrink.

In the above equation, the diffusion coefficient D can be set to 1 since we can always rescale the time properly. Then, combining Eqs. (1) and (2), we have the diffusion equation

$$\frac{\partial \rho}{\partial t} = \Delta \rho \quad (3)$$

and the expression of velocity

$$\mathbf{v} = -\frac{\nabla \rho}{\rho}. \quad (4)$$

Since the velocity \mathbf{v} is independent of the absolute scale of ρ , the update of the velocity field is stable. Note that any tracer $\mathbf{x}(t)$ will move with the velocity $\mathbf{v}(\mathbf{x}(t), t)$. We have the tracer displacement

$$\mathbf{x}(t) = \mathbf{x}(0) + \int_0^t \mathbf{v}(\mathbf{x}(\tau), \tau) d\tau. \quad (5)$$

After the diffusion, the density ρ will be equal at every position in the deformed domain and hence $\nabla \rho \equiv 0$. This means that $\lim_{t \rightarrow \infty} \mathbf{x}(t)$ will exist for any tracer $\mathbf{x}(t)$ and it will give the stable position of the corresponding part of the domain (see Fig. 2 for an illustration). Note that since the density function is positive, the transformation has a non-vanishing Jacobian (see [1] for details). Also, to avoid infinite expansion of the domain, Gastner and Newman [1] put a large auxiliary rectangular region as the “sea” outside the domain D and set the density at the sea as the average of the density at D . The density diffusion and mapping computation are performed on the entire region including both D and the auxiliary sea. This effectively constrains the diffusion so that the actual domain of interest can undergo shape deformations based on the prescribed density information without expanding infinitely.

While the density-equalizing mapping approach was originally developed for sociological data visualization, it was later extended and utilized as a method for surface mapping and parameterization [10].

3. Toroidal density-equalizing maps

Consider a torus

$$\mathcal{T} = \left\{ (X, Y, Z) \in \mathbb{R}^3 \mid \left(\sqrt{X^2 + Y^2} - R \right)^2 + Z^2 = r^2 \right\},$$

where R and r are the prescribed major and minor radii with $R > r > 0$. Let $\rho(X, Y, Z)$ be a density function defined on \mathcal{T} . Our goal is to compute a density-equalizing map $f : \mathcal{T} \rightarrow \mathcal{T}$ that produces a deformation on the toroidal domain based on some prescribed density. More specifically, let ρ be a density function on the torus \mathcal{T} defined as the “population” per unit area. Here, the “population” is some positive quantity (analogous to the human population in the original cartogram creation problem [1]) that we prescribe to create a desired shape deformation effect. In the discrete case, we represent the torus \mathcal{T} as a triangulated surface $(\mathcal{V}, \mathcal{E}, \mathcal{F})$ where \mathcal{V} is the set of vertices, \mathcal{E} is the set of edges and \mathcal{F} is the set of triangular faces. Let $\mathcal{V} = \{v_i\}_{i=1}^{|\mathcal{V}|}$, $\mathcal{E} = \{e_j\}_{j=1}^{|\mathcal{E}|}$ and $\mathcal{F} = \{T_m\}_{m=1}^{|\mathcal{F}|}$. The density ρ is discretized on \mathcal{T} as:

$$\rho_T(T_m) = \frac{P(T_m)}{\text{Area}(T_m)},$$

where $P(T_m)$ is the prescribed population function on the triangle T_m .

Intuitively, one may directly extend the computation in Section 2 to the toroidal case by solving the diffusion equation on the torus and performing the vertex position update accordingly. However, the density gradient $\nabla \rho$ in \mathbb{R}^3 may lead to a change in the toroidal geometry. Specifically, under the vertex update, some vertices may no longer lie on the torus \mathcal{T} and hence an extra projection

step would be needed, which would lead to numerical errors and discrepancies between the density diffusion process and the shape deformations. Noticing that the torus is a parametric surface and can be easily represented by two angular coordinates, here we consider solving the density diffusion and shape deformation problems on a planar domain with periodic boundary conditions, thereby effectively mitigating the above-mentioned issues and simplifying the computational procedure.

We first define the toroidal projection $\phi : [0, 2\pi R) \times [-\pi r, \pi r) \rightarrow \mathcal{T}$ as follows:

$$\begin{aligned}\phi(u, v) &= (X(u, v), Y(u, v), Z(u, v)) \\ &= \left(\left(R + r \cos \frac{v}{r} \right) \cos \frac{u}{R}, \left(R + r \cos \frac{v}{r} \right) \sin \frac{u}{R}, r \sin \frac{v}{r} \right).\end{aligned}\quad (6)$$

Note that ϕ gives a 1–1 correspondence between a rectangular domain with width $2\pi R$ and height $2\pi r$ and the torus \mathcal{T} . Also, it can be naturally extended for other values of u, v outside the domain using the periodicity of the sine and cosine functions. We remark that here we use $[0, 2\pi R) \times [-\pi r, \pi r)$ instead of the usual parameter domain with width 2π and height 2π so that the planar domain better resembles the geometry of the given torus. Also, we use $[-\pi r, \pi r)$ instead of $[0, 2\pi r)$ so that the top and bottom boundaries are mapped to the innermost loop of the torus. We remark that the inverse toroidal projection $\phi^{-1} : \mathcal{T} \rightarrow [0, 2\pi R) \times [-\pi r, \pi r)$ can also be explicitly expressed, with $\phi^{-1}(X, Y, Z) = (u(X, Y, Z), v(X, Y, Z))$ where

$$u(X, Y, Z) = \begin{cases} R \sin^{-1} \left(\frac{Y}{\sqrt{X^2 + Y^2}} \right) & \text{if } X \geq 0 \text{ and } Y \geq 0, \\ R \left(2\pi + \sin^{-1} \left(\frac{Y}{\sqrt{X^2 + Y^2}} \right) \right) & \text{if } X \geq 0 \text{ and } Y < 0, \\ R \left(\pi - \sin^{-1} \left(\frac{Y}{\sqrt{X^2 + Y^2}} \right) \right) & \text{otherwise,} \end{cases}$$

with the range of the principal values of \sin^{-1} being $[-\pi/2, \pi/2]$, and v can be expressed in a similar manner:

$$v(X, Y, Z) = \begin{cases} r \sin^{-1} \left(\frac{Z}{r} \right) & \text{if } X^2 + Y^2 \geq R^2, \\ r \left(\pi - \sin^{-1} \left(\frac{Z}{r} \right) \right) & \text{if } X^2 + Y^2 < R^2 \text{ and } Z > 0, \\ -r \left(\pi + \sin^{-1} \left(\frac{Z}{r} \right) \right) & \text{otherwise.} \end{cases}$$

Now, we consider solving for the toroidal mapping f via the planar domain instead of on the toroidal surface \mathcal{T} . We denote the initial position of all vertices on the planar domain as $\mathbf{x}^{(0)}(v_i) = \phi^{-1}(v_i)$ and hence attain the initial triangle on the planar domain $\bar{T}^{(0)} = [\mathbf{x}^{(0)}(v_i), \mathbf{x}^{(0)}(v_j), \mathbf{x}^{(0)}(v_k)]$ corresponding to $T = [v_i, v_j, v_k] \in \mathcal{F}$. It is noteworthy that the toroidal projection ϕ is not an isometric mapping. Therefore, to ensure that the density diffusion on the planar domain is consistent with the density diffusion on the torus, we need to work with a density function that takes the difference between the planar domain and the torus into consideration. To achieve this, we define the initial modified density $\tilde{\rho}_{\bar{T}}^{(0)}$ on the planar domain in vector form as

$$\tilde{\rho}_{\bar{T}}^{(0)}(m) = \frac{P(T_m)}{\text{Area}(T_m)}, \quad (7)$$

where $T_m \in \mathcal{F}$. Here, note that the area factor is computed based on the area of the mapped triangle T_m on the torus instead of the triangle $\bar{T}^{(0)} = [\phi^{-1}(v_i), \phi^{-1}(v_j), \phi^{-1}(v_k)]$ on the planar domain. This ensures that while the density diffusion process and the associated vertex updates are performed on the plane subsequently, the resulting map will satisfy the desired shape deformation effect on the torus \mathcal{T} . After getting the initial face-based modified density $\tilde{\rho}_{\bar{T}}^{(0)}$, we can compute the initial vertex-based modified density vector:

$$\tilde{\rho}_v^{(0)}(i) = \frac{\sum_{T_m \in \mathcal{N}_{\mathcal{F}}(v_i)} \text{Area}(T_m) \tilde{\rho}_{\bar{T}}^{(0)}(m)}{\sum_{T_m \in \mathcal{N}_{\mathcal{F}}(v_i)} \text{Area}(T_m)}, \quad (8)$$

where $\mathcal{N}_{\mathcal{F}}(v_i)$ is the 1-ring face neighborhood of the vertex v_i .

Now, we focus on performing the density diffusion and mapping processes on the plane based on the modified density using an iterative scheme. Let δt be a chosen step size, and denote the position function of the vertices and the corresponding planar triangle at time $t = k\delta t$ by $\mathbf{x}^{(k)}$ and $\bar{T}^{(k)} = [\mathbf{x}^{(k)}(v_i), \mathbf{x}^{(k)}(v_j), \mathbf{x}^{(k)}(v_k)]$ respectively for $k \in \mathbb{N}$.

We first solve the diffusion equation (3)

$$\frac{\partial \rho}{\partial t} = \Delta \rho.$$

In a discrete triangulated mesh, the Laplacian is discretized as

$$\Delta = -A^{-1}L \quad (9)$$

where A is a $|\mathcal{V}| \times |\mathcal{V}|$ diagonal matrix (called the lumped area matrix) with its diagonal entries given by

$$A_{ii} = \frac{1}{3} \sum_{T \in \mathcal{N}_{\mathcal{F}}(v_i)} \text{Area}(T),$$

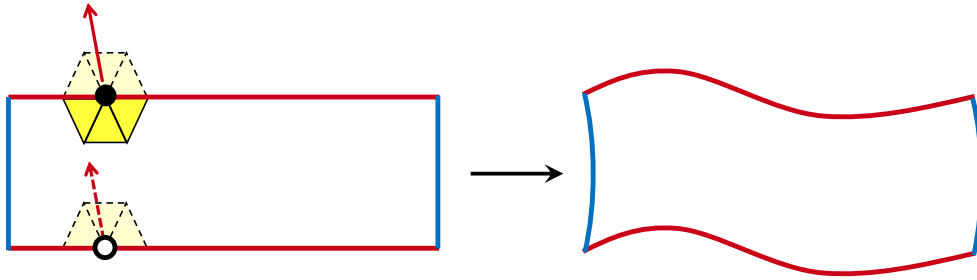


Fig. 3. An illustration of the periodic boundary constraints in the planar density diffusion and mapping process. Throughout the planar density diffusion and mapping process, periodic boundary constraints need to be enforced for both the top and bottom boundaries (red) and both the left and right boundaries (blue). Specifically, for every pair of corresponding boundary vertices (the black dot and the white dot), a virtual copy of the neighboring nodes and triangles will be considered in the density diffusion process so that the density information can be exchanged along the boundaries. The boundaries are then updated consistently so that they only differ by a translation, which ensures that they will be mapped back to a consistent location on the torus under the toroidal projection.

and L is a $|\mathcal{V}| \times |\mathcal{V}|$ sparse matrix (called the cotangent Laplacian [27]) with

$$L_{ij} = \begin{cases} -\frac{1}{2}(\cot \alpha_{ij} + \cot \beta_{ij}) & \text{if } i \neq j \text{ and } v_j \in \mathcal{N}_{\mathcal{V}}(v_i), \\ -\sum_{k=1}^{|\mathcal{V}|} L_{ik} & \text{if } i = j, \\ 0 & \text{otherwise,} \end{cases}$$

where $\mathcal{N}_{\mathcal{V}}(v_i)$ is the 1-ring vertex neighborhood of the vertex v_i , and α_{ij}, β_{ij} are two angles opposite to the edge $[\bar{v}_i, \bar{v}_j] \in \mathcal{E}$ on the planar domain. We can then solve the diffusion equation with Eq. (9) using the semi-discrete backward Euler method iteratively:

$$\frac{\tilde{\rho}_v^{(n+1)} - \tilde{\rho}_v^{(n)}}{\delta t} = -(A^{(n)})^{-1} L^{(n)} \tilde{\rho}_v^{(n+1)} \iff \tilde{\rho}_v^{(n+1)} = (A^{(n)} + L^{(n)} \delta t)^{-1} A^{(n)} \tilde{\rho}_v^{(n)}, \quad (10)$$

where $n \geq 0$ is the iteration number, $\tilde{\rho}_v^{(k)}$ is the modified density vector of vertex at time $t = k \delta t$, and $A^{(k)}, L^{(k)}$ are dependent on $\bar{T}^{(k)}$.

Recall that in the original density-equalizing mapping approach [1], an auxiliary “sea” is set surrounding the actual planar domain to avoid infinite expansion of the domain and allow it to change freely in shape. Now, note that in our problem formulation for toroidal density-equalizing maps, the density diffusion process occurs on the plane, and the planar deformation result will be mapped back to the toroidal surface \mathcal{T} via the toroidal projection ϕ . Also, one can easily see that the top and bottom boundaries of the initial planar domain will be mapped to the same curve on \mathcal{T} under ϕ , as we have

$$\begin{aligned} & \phi(u, v + 2\pi r) \\ &= \left(\left(R + r \cos \frac{v + 2\pi r}{r} \right) \cos \frac{u}{R}, \left(R + r \cos \frac{v + 2\pi r}{r} \right) \sin \frac{u}{R}, r \sin \frac{v + 2\pi r}{r} \right) \\ &= \phi(u, v). \end{aligned}$$

Similarly, the left and right boundaries of the initial domain will be mapped to the same curve on \mathcal{T} under ϕ as we have

$$\begin{aligned} & \phi(u + 2\pi R, v) \\ &= \left(\left(R + r \cos \frac{v}{r} \right) \cos \frac{u + 2\pi R}{R}, \left(R + r \cos \frac{v}{r} \right) \sin \frac{u + 2\pi R}{R}, r \sin \frac{v}{r} \right) \\ &= \phi(u, v). \end{aligned}$$

Therefore, while the planar domain should change its overall shape under the density diffusion and shape deformation process, it is desired that the consistency between the boundaries when mapped back to the torus under toroidal projection will be preserved throughout the process. To achieve this, instead of introducing an auxiliary “sea” as in [1], here we only need to consider the actual planar domain and modify the boundary constraints when computing the vertex-based density gradient and performing the vertex update.

Specifically, when solving the diffusion equation in Eq. (10), we identify the opposite boundaries of the domain to ensure that the density information can be exchanged along the boundaries. This involves considering a virtual copy of the neighboring nodes and triangles for every pair of corresponding boundary vertices (see Fig. 3 for an illustration) in the construction of the lumped area matrix $A^{(k)}$ and cotangent Laplacian $L^{(k)}$. In practice, after computing the entries in a row in $A^{(k)}, L^{(k)}$ associated with a vertex at the left or bottom boundary, we modify $A^{(k)}, L^{(k)}$ by further adding the entries to the row associated with its corresponding vertex at the right or top boundary.

After getting the updated density $\tilde{\rho}_v^{(n+1)}$, we copy the values of $\tilde{\rho}_v^{(n+1)}$ at the right and top boundary vertices to their counterparts at the left and bottom boundaries. We then put all the planar triangle $\bar{T}^{(n)}$ on the x - y plane of \mathbb{R}^3 and compute the planar face-based

density gradient $\nabla \tilde{\rho}_T^{(n)}$ at time $t = n\delta t$ in matrix form (see [10] for details):

$$\nabla \tilde{\rho}_T^{(n)}(m) = \frac{\mathbf{n}_m \times (\tilde{\rho}_v^{(n+1)}(i)e_{jk}^{(n)} + \tilde{\rho}_v^{(n+1)}(j)e_{ki}^{(n)} + \tilde{\rho}_v^{(n+1)}(k)e_{ij}^{(n)})}{2\text{Area}(\bar{T}_m^{(n)}), \quad (11)$$

where $\nabla \tilde{\rho}_T^{(n)}(m)$ is the m th row of the matrix corresponding to the gradient of the planar face $\bar{T}_m^{(n)} = [\mathbf{x}^{(n)}(v_i), \mathbf{x}^{(n)}(v_j), \mathbf{x}^{(n)}(v_k)]$, \mathbf{n}_m is the unit upward normal of the triangle $\bar{T}_m^{(n)}$ in \mathbb{R}^3 , $\tilde{\rho}_v^{(n)}(q)$ is the density values at v_q and $e_{pq}^{(n)} = \mathbf{x}^{(n)}(v_q) - \mathbf{x}^{(n)}(v_p)$. Note that $\nabla \tilde{\rho}_T^{(n)}(m)$ is still within x - y plane. So we can put the gradient back to the planar domain by reducing its z -coordinate and attain a $|\mathcal{V}| \times 2$ matrix $\nabla \tilde{\rho}_T^{(n)}$. Then, we can get the vertex-based density gradient $\nabla \tilde{\rho}_v^{(n)}$ from the face-based density gradient $\nabla \tilde{\rho}_T^{(n)}$ via a simple conversion:

$$\nabla \tilde{\rho}_v^{(n)} = M^{(n)} \nabla \tilde{\rho}_T^{(n)}, \quad (12)$$

where $M^{(n)}$ is a $|\mathcal{V}| \times |\mathcal{F}|$ conversion matrix with

$$M_{ij}^{(n)} = \begin{cases} \frac{\text{Area}(T_j^{(n)})}{\sum_{T \in \mathcal{N}_F(v_i)} \text{Area}(T^{(n)})} & \text{if } T_j^{(n)} \text{ is incident to } v_i, \\ 0 & \text{otherwise.} \end{cases}$$

Here, $T^{(n)} = [\phi(\mathbf{x}^{(n)}(v_i)), \phi(\mathbf{x}^{(n)}(v_j)), \phi(\mathbf{x}^{(n)}(v_k))]$ is the triangle on the torus at time $t = n\delta t$. Analogous to the construction of $A^{(k)}, L^{(k)}$, here we also encode the periodicity of the domain in the construction of $M^{(k)}$ by modifying the rows of it corresponding to the boundary vertices.

Now, from the vertex-based density gradient $\nabla \tilde{\rho}_v^{(n)}$, we can get the velocity vector similar to Eq. (4) at v_i at time $t = n\delta t$:

$$\mathbf{v}_i^{(n)} = -\frac{\nabla \tilde{\rho}_v^{(n)}(i)}{\tilde{\rho}_v^{(n)}(i)}. \quad (13)$$

where $\tilde{\rho}_v^{(n)}(i), \nabla \tilde{\rho}_v^{(n)}(i)$ are the vertex-based density and gradient related to v_i . We then use Eq. (5) in the discrete case to update the planar position of v_i on the plane:

$$\mathbf{x}^{(n+1)}(v_i) = \mathbf{x}^{(n)}(v_i) + \mathbf{v}_i^{(n)} \delta t, \quad (14)$$

As discussed above, there is a consistency between opposite boundaries in the initial planar domain as they correspond to the same curves under the toroidal projection. Because of the periodicity enforced in the above-mentioned diffusion equation solver and density gradient computation, the periodicity of the two pairs of boundaries in terms of their vertex positions under the vertex position update in Eq. (14) is automatically satisfied (see Fig. 3 for an illustration). Specifically, suppose $(x_{\text{top}}, y_{\text{top}})$ and $(x_{\text{bottom}}, y_{\text{bottom}})$ are two vertices on the top and bottom boundaries of the planar domain such that their corresponding positions on the torus \mathcal{T} are identical, i.e., $\phi(x_{\text{top}}, y_{\text{top}}) = \phi(x_{\text{bottom}}, y_{\text{bottom}})$. Under the vertex position update, their positions on the plane will only differ by a translation:

$$\begin{cases} x_{\text{top}} &= x_{\text{bottom}}, \\ y_{\text{top}} &= y_{\text{bottom}} + 2\pi r. \end{cases}$$

Similarly, suppose $(x_{\text{left}}, y_{\text{left}})$ and $(x_{\text{right}}, y_{\text{right}})$ are two vertices on the left and right boundaries of the planar domain such that their corresponding positions on \mathcal{T} are identical. Under the vertex position update, we will have:

$$\begin{cases} x_{\text{right}} &= x_{\text{left}} + 2\pi R, \\ y_{\text{right}} &= y_{\text{left}}. \end{cases}$$

In other words, while the planar domain can change its shape from a rectangle to some other planar shape, the periodicity between the top and bottom boundaries and between the left and right boundaries is always preserved.

After performing the vertex update above, we follow the idea in [13] and include a few extra steps for correcting potential mesh overlaps and recoupling the density and the deformation at the end of each iteration. Specifically, one can consider the mapping between the initial planar parameterization D_0 and the current deformation result D_n as a quasi-conformal map $g : D_0 \rightarrow D_n$. Then, the bijectivity of the mapping g can be checked using the Beltrami coefficient μ . In case there are mesh fold-overs, we will have $\|\mu\|_\infty \geq 1$. Following the procedure in [13], one can perform a simple truncation on μ to get an updated Beltrami coefficient $\tilde{\mu}$ to enforce $\|\tilde{\mu}\|_\infty < 1$, followed by solving a sparse linear system that updates the vertex positions. This approach allows us to obtain an updated mapping result \tilde{g} with a positive Jacobian, thereby effectively correcting local mesh fold-overs caused by large deformations induced by extreme density gradients. More details are provided in [13]. Furthermore, in our case, by fixing the boundary points, we can ensure that the periodicity will remain preserved under the correction step. As shown by our experimental results, even with the above-mentioned mesh overlap correction scheme included, the method can still converge to a steady state as time increases. See Section 5 for the results and the relevant discussions.

Also, the density-deformation recoupling scheme [13] aims to reduce numerical errors and discrepancies between the shape deformation and the density flow by re-defining the density using the updated vertex positions for the next iteration. In our case, we follow the same procedure and re-define the face-based density based on $\bar{T}_m^{(n+1)} = [\mathbf{x}^{(n+1)}(v_i), \mathbf{x}^{(n+1)}(v_j), \mathbf{x}^{(n+1)}(v_k)]$ as

$$\tilde{\rho}_T^{(n+1)}(m) = \frac{P(T_m)}{\text{Area}(T_m^{(n+1)})} \quad (15)$$

using the given population P and the latest mapping result $\mathbf{x}^{(n+1)}$ at the end of each iteration. Then we use a similar method in Eq. (12) to recouple the vertex-based density

$$\bar{\rho}_v^{(n+1)} = M^{(n+1)} \bar{\rho}_{\bar{T}}^{(n+1)}. \quad (16)$$

We can then repeat the above process until the density error $E(\bar{\rho}_v^{(n+1)}) = \frac{\text{std}(\bar{\rho}_v^{(n+1)})}{\text{mean}(\bar{\rho}_v^{(n+1)})}$ is less than a prescribed error threshold ϵ or the number of iterations n reaches a prescribed threshold n_{\max} .

Finally, we can map the planar deformation result onto the torus \mathcal{T} using the toroidal projection ϕ in Eq. (6). The resulting displacements of all vertices on \mathcal{T} relative to their initial position on \mathcal{T} give the desired density-equalizing map $f : \mathcal{T} \rightarrow \mathcal{T}$. The proposed TDEM algorithm is summarized in Algorithm 1.

Algorithm 1: Toroidal density-equalizing map (TDEM)

Data: A toroidal surface \mathcal{T} with major radius R and minor radius r , a prescribed population function P defined on every triangular face, the step size δt , the error threshold ϵ , and the maximum number of iterations n_{\max} .

Result: A toroidal density-equalizing map $f : \mathcal{T} \rightarrow \mathcal{T}$.

- 1 Use the inverse toroidal projection ϕ^{-1} to map \mathcal{T} onto a planar domain $[0, 2\pi R) \times [-\pi r, \pi r)$ to get the initial position $\mathbf{x}^{(0)}$;
 - 2 Calculate the initial modified density $\bar{\rho}_{\bar{T}}^{(0)}$ and $\bar{\rho}_v^{(0)}$ using Eq. (7) and Eq. (8) and set $n = 0$;
 - 3 **while** $E(\bar{\rho}_v^{(n)}) \geq \epsilon$ and $n \leq n_{\max}$ **do**
 - 4 Solve the diffusion equation in Eq. (10) to get the updated vertex-based density $\bar{\rho}_v^{(n+1)}$;
 - 5 Calculate the modified density gradient $\nabla \bar{\rho}_{\bar{T}}^{(n)}$ and $\nabla \bar{\rho}_v^{(n)}$ using Eq. (11)–(12);
 - 6 Compute the velocity field $\mathbf{v}^{(n)}$ using Eq. (13);
 - 7 Update the planar vertex position $\mathbf{x}^{(n+1)}$ using Eq. (14);
 - 8 Apply the mesh overlap correction scheme;
 - 9 Recouple the vertex-based density $\bar{\rho}_v^{(n+1)}$ using Eq. (15)–(16);
 - 10 Update n by $n + 1$;
 - 11 Denote the final planar vertex position mapping result as $\mathbf{x} : \mathcal{T} \rightarrow \mathbb{R}^2$;
 - 12 Apply the toroidal projection ϕ to map the planar mapping result onto \mathcal{T} ;
 - 13 The desired toroidal map is given by $f = \phi \circ \mathbf{x}$;
-

4. Toroidal density-equalizing parameterization of genus-one surfaces

Recall that the surface parameterization problem aims to map a given surface onto a simple standardized domain with some given mapping criteria. As the above toroidal density-equalizing mapping method is capable of creating a shape deformation on the torus based on some prescribed population functions, it is natural to extend the TDEM method for the parameterization of genus-one surfaces onto a given torus.

More specifically, given a genus-one surface S , a prescribed population defined on it, and a target toroidal surface \mathcal{T} with major radius R and minor radius r , our goal is to compute a toroidal parameterization $f : S \rightarrow \mathcal{T}$ that achieves the desired area change effects encoded in the prescribed population.

Our proposed toroidal parameterization method is outlined in Fig. 4. We first find an initial parameterization $h : S \rightarrow \mathcal{T}$ that maps the input surface S onto the prescribed torus \mathcal{T} . The initial parameterization can be computed using any existing methods. In particular, a simple way is to slice S along two cut paths to get a simply connected open surface and map it onto a planar rectangular domain with periodic boundary conditions. In practice, we construct the initial toroidal parameterization by applying the rectangular conformal mapping method [28] with a modification of the boundary conditions as in [29]. Specifically, the method in [29] enforced the periodicity of the left and right boundaries, while here we enforce the periodicity for both the left and right boundaries and the top and bottom boundaries so that the mapping result gives a seamless initial toroidal parameterization. We remark that since the initial parameterization involves mapping the sliced mesh onto a rectangular domain, it is desirable to choose two geodesic cut paths along the edges of the triangulated surface that are as perpendicular to each other as possible, which allows us to reduce the geometric distortions in the initial mapping result. Nevertheless, other choices of non-perpendicular and non-geodesic cut paths can also be considered in practice. More detailed discussions and experiments will be covered in Section 5.2.

After getting the initial toroidal parameterization, we can apply the inverse toroidal projection ϕ^{-1} to map the torus onto the plane. We can then apply the proposed TDEM method (Algorithm 1) to compute a toroidal density-equalizing map $g : \mathcal{T} \rightarrow \mathcal{T}$ via a planar mapping process with the periodic conditions satisfied. Here, the initial density $\bar{\rho}$ for the TDEM method is given by $\bar{\rho}(\hat{T}) = \frac{P(\hat{T})}{\text{Area}(\hat{T})}$, where \hat{T} is a triangular face on the torus \mathcal{T} associated with the triangular face T on the input surface S , i.e., $\hat{T} = h(T)$, and P is the prescribed population function controlling the mapping effect.

Finally, the composition of the above mappings gives the desired toroidal parameterization $f = g \circ h$. The proposed toroidal density-equalizing parameterization method is summarized in Algorithm 2.

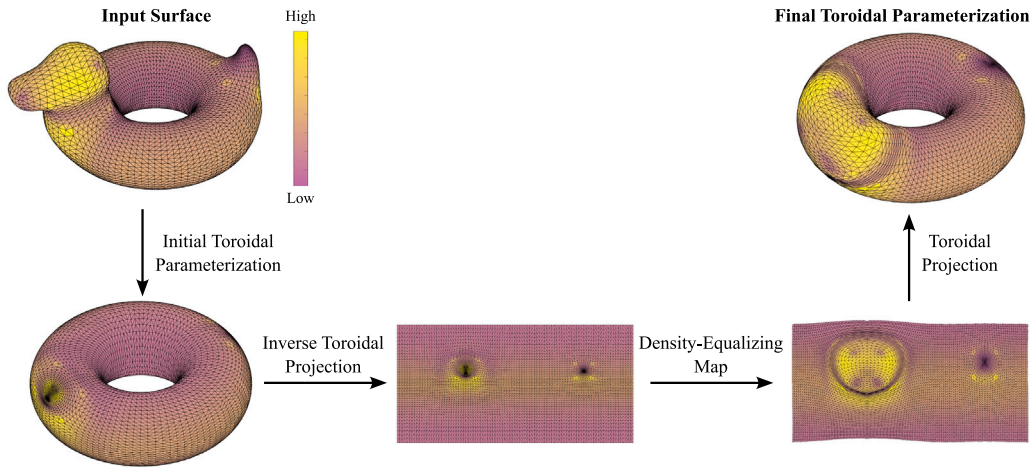


Fig. 4. Outline of the proposed toroidal density-equalizing parameterization method. Given a genus-one surface with some prescribed population, we first compute an initial parameterization of it onto a torus. Then, we apply the inverse toroidal projection to map the torus onto the plane. We then apply our TDEM algorithm to obtain the deformed planar map with the periodic condition satisfied. Finally, we apply the toroidal projection to map the planar mapping result onto the torus, yielding the desired toroidal density-equalizing parameterization.

Algorithm 2: Toroidal density-equalizing parameterization of genus-one surfaces

Data: A genus-one surface S , the target toroidal surface \mathcal{T} , a prescribed population P , the step size δt , the error threshold ϵ , and the maximum number of iterations n_{\max} .

Result: A toroidal parameterization $f : S \rightarrow \mathcal{T}$.

- 1 Compute an initial parameterization $h : S \rightarrow \mathcal{T}$;
 - 2 Apply the TDEM algorithm with the prescribed population P , the step size δt , the error threshold ϵ , and the maximum number of iterations n_{\max} to obtain a toroidal map $g : \mathcal{T} \rightarrow \mathcal{T}$;
 - 3 The desired toroidal density-equalizing parameterization is given by $f = g \circ h$;
-

As a particular case, the proposed toroidal parameterization algorithm can be used for producing toroidal area-preserving parameterization. Specifically, we follow the approach in [10] and define the input population as exactly the area of each triangular face of S . Then, the initial density in the TDEM method will be given by $\tilde{\rho}(T) = \frac{\text{Area}(T)}{\text{Area}(h(T))}$, where T is a triangular face on S . By applying the TDEM algorithm to the torus based on $\tilde{\rho}$, the resulting map will give a constant final density of $\frac{\text{Area}(T)}{\text{Area}(g \circ h(T))} = \frac{\text{Area}(T)}{\text{Area}(f(T))}$. In other words, all triangles will be enlarged or shrunk precisely on the torus \mathcal{T} according to their original size on S , thereby yielding an area-preserving parameterization.

As a remark, in the proposed algorithm, a target toroidal surface is prescribed as input. As shown in the experimental results later, our algorithm is applicable to different target toroidal surfaces with different major and minor radii R and r . One may also set the shape of the target toroidal surface based on the geometry of the input genus-1 surface. More details will be covered in Section 5.2.

5. Experimental results

In this section, we present numerical experiments to evaluate the performance of our proposed toroidal density-equalizing map and toroidal parameterization methods. Various genus-one surface models from online mesh repositories [30–33] are used in our experiments. The proposed algorithms are implemented in MATLAB R2021a. All experiments are performed on a Windows Computer with an Intel i9-12900 processor with 32 GB RAM. In all our experiments, we set the time step size $\delta t = 0.1$ (other choices will also be examined later). The error threshold is set to be $\epsilon = 10^{-2}$, and the maximum number of iterations is set to be $n_{\max} = 500$.

5.1. Toroidal density-equalizing map

We start by considering different density functions ρ on a prescribed toroidal surface and applying the TDEM algorithm (Algorithm 1).

In the first example (Fig. 5), we consider a torus with major radius $R = 3$ and minor radius $r = 1$. We define the input population as $P(T) = (2 - \cos(u))\text{Area}(T)$, where (u, v) is the face centroid of the triangle T under the inverse toroidal projection ϕ^{-1} . This population function only involves variations along the toroidal direction but not the poloidal direction on the torus. Equivalently, there are only variations in the x -direction in the planar domain but not in the y -direction. We can easily see that the planar mapping does not produce any overall shape change, and the boundary vertices only slice along the boundaries. In the final TDEM result, we can also see that the shape deformation only involves enlargements and shrinkages along the toroidal direction.

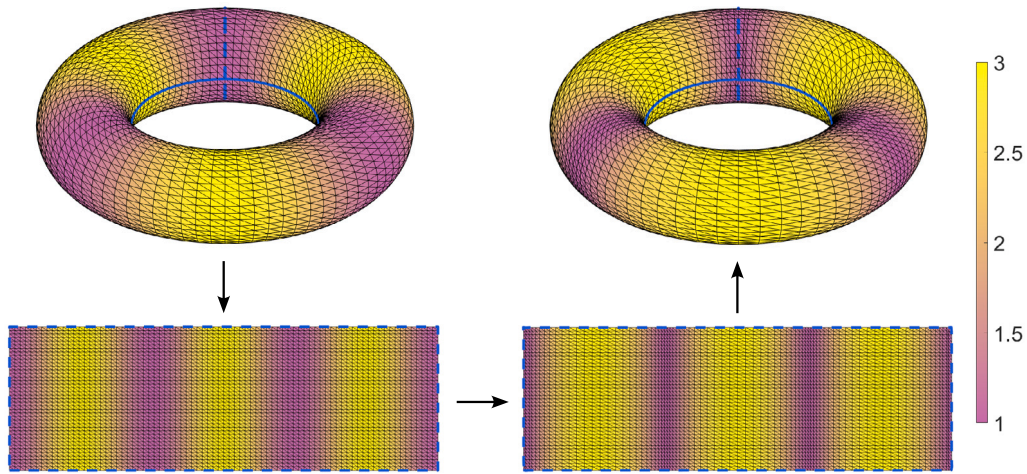


Fig. 5. Mapping a torus with the prescribed population $P(T) = (2 - \cos(u))\text{Area}(T)$, where (u, v) is the face centroid of the triangle T under the inverse toroidal projection ϕ^{-1} . The top-left figure panel shows the original toroidal surface. The bottom-left panel shows the planar representation of the original toroidal surface under ϕ^{-1} . The bottom-right panel shows the planar mapping result. The top-right panel shows the final TDEM result. All surfaces are color-coded with the initial density $\bar{\rho}_T^{(0)}$. The blue dotted lines represent the cut paths.

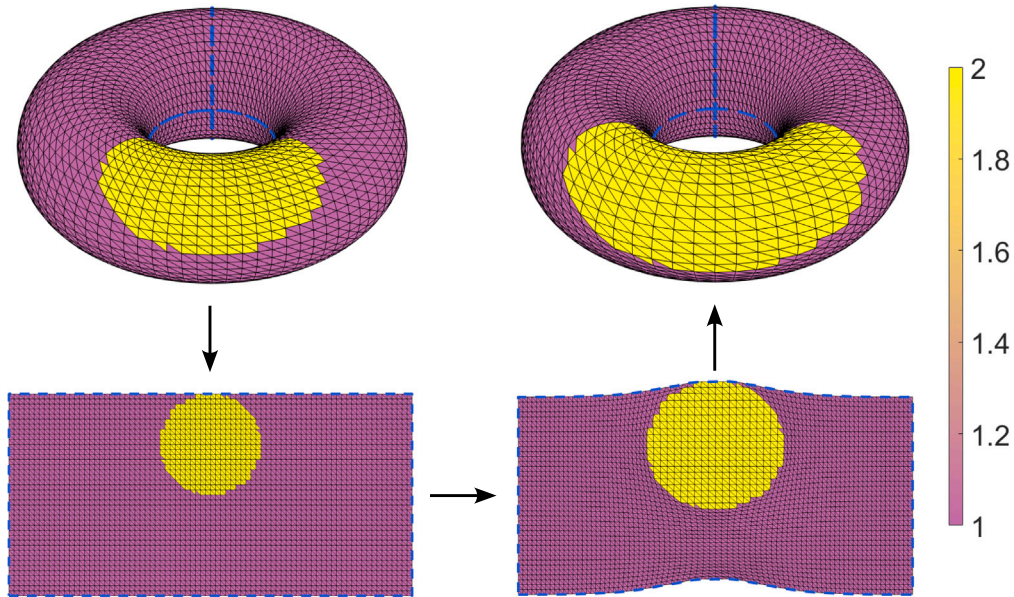


Fig. 6. Mapping a torus with the prescribed population function involving a circular region with a higher population. The top-left figure panel shows the original toroidal surface. The bottom-left panel shows the planar representation of the original toroidal surface under ϕ^{-1} . The bottom-right panel shows the planar mapping result. The top-right panel shows the final TDEM result. All surfaces are color-coded with the initial density $\bar{\rho}_T^{(0)}$. The blue dotted lines represent the cut paths.

In the second example (Fig. 6), we consider a torus with $(R, r) = (2, 1)$ and an input population P where $P(T) = 2 \cdot \text{Area}(T)$ for the triangles corresponding to a ball centering at $(\pi R, \frac{\pi}{2}r)$ with the radius $\frac{r}{2}$ in the planar domain and $P(T) = \text{Area}(T)$ otherwise. This population involves variations that produce boundary deformations in only one boundary pair of the planar domain. It can be observed in the planar mapping result that the top and bottom parts of the domain are significantly deformed in a periodic manner, while the overall shapes of the left and right boundaries are unchanged. In the final TDEM mapping result, we can see a clear deformation on the torus involving changes in both the toroidal and poloidal directions, where the high-density regions are expanded and the low-density regions are shrunk.

Next, we consider an example (Fig. 7) for which the prescribed population is $(1.2 - \sin(u)\sin(v))\text{Area}(T)$ on a torus with $(R, r) = (3, 1)$. Because of the choice of the population, the density involves variations that produce boundary deformations in both boundary pairs of the planar domain. As shown in the planar mapping result, both boundary pairs are deformed consistently to

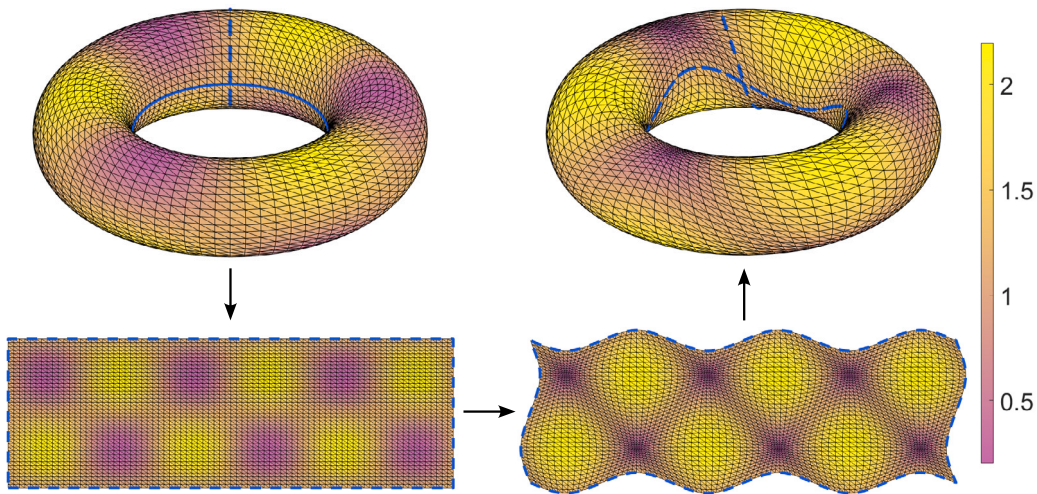


Fig. 7. Mapping a torus with the prescribed population $P(T) = (1.2 - \sin(u) \sin(v)) \text{Area}(T)$, where (u, v) is the face centroid of every triangle T under the inverse toroidal projection ϕ^{-1} . The top-left figure panel shows the original toroidal surface. The bottom-left panel shows the planar representation of the original toroidal surface under ϕ^{-1} . The bottom-right panel shows the planar mapping result. The top-right panel shows the final TDEM result. All surfaces are color-coded with the initial density $\bar{\rho}_T^{(0)}$. The blue dotted lines represent the cut paths.

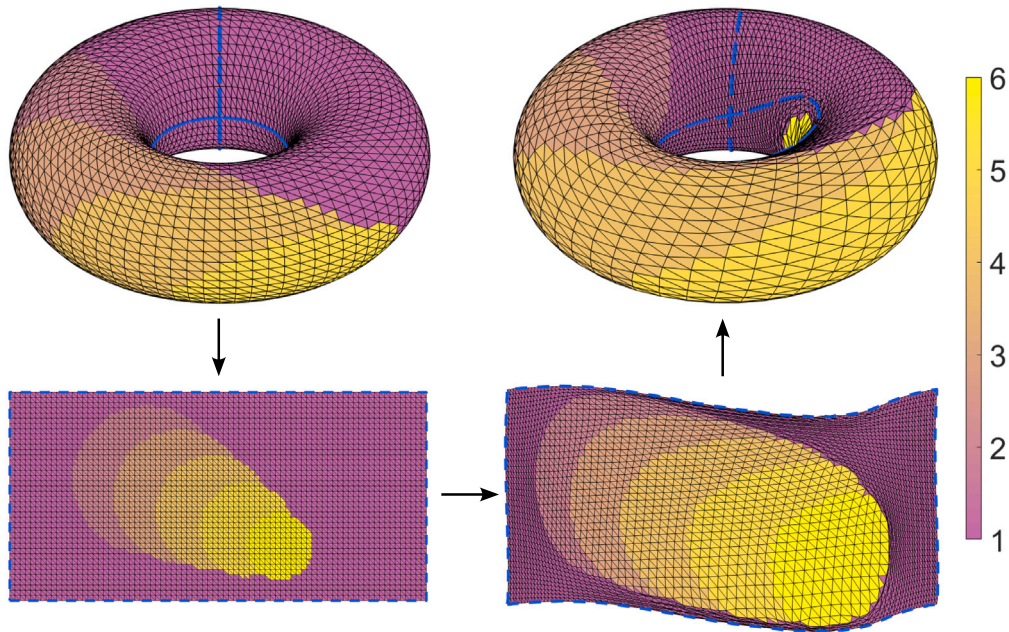


Fig. 8. Mapping a torus with a more unsmooth density distribution. The top-left figure panel shows the original toroidal surface. The bottom-left panel shows the planar representation of the original toroidal surface under ϕ^{-1} . The bottom-right panel shows the planar mapping result. The top-right panel shows the final TDEM result. All surfaces are color-coded with the initial density $\bar{\rho}_T^{(0)}$. The blue dotted lines represent the cut paths.

achieve density equalization. In the final TDEM result, it can also be observed that the vertices are deformed in multiple directions on the torus.

Note that the above examples involve some simple or smooth density distributions over the entire domain. It is natural to ask whether our TDEM method also works for more unsmooth densities. Here, we consider a more complicated example (Fig. 8) with multiple overlapping circular regions with a higher population at the bottom right of the planar domain, while the populations at all other parts are uniform. In this case, it is expected that the bottom right part will expand because of the higher-density regions. In the mapping result, we can see that indeed the diffusion process expands the bottom boundary and hence results in the top shrinking. Besides visualizing the mapping effect, we can also assess the mapping result by computing the density distributions

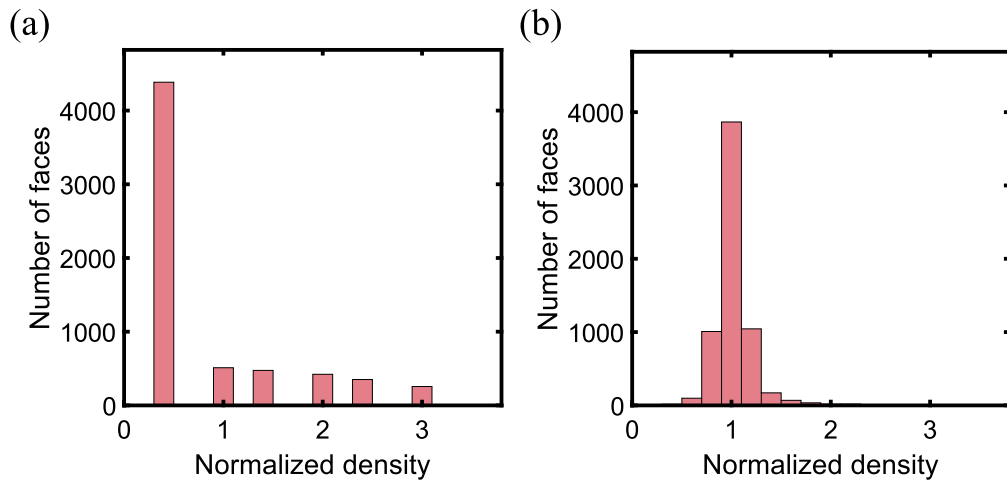


Fig. 9. The normalized initial and final density distributions in the example in Fig. 8. (a) The normalized initial density $\bar{\rho}_{\text{initial}} = \frac{\rho_{\text{initial}}}{\text{mean}(\rho_{\text{initial}})}$. (b) The normalized final density $\bar{\rho}_{\text{final}} = \frac{\rho_{\text{final}}}{\text{mean}(\rho_{\text{final}})}$.

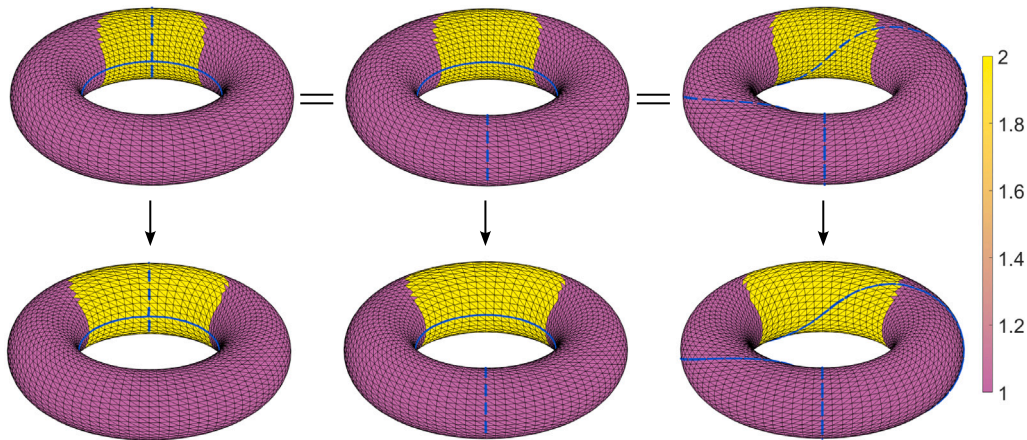


Fig. 10. An example of mapping three toroidal surfaces with different cut paths. The upper row shows three toroidal surfaces with equivalent density distributions. The lower row shows the final TDEM results. The blue dotted lines represent the cut paths.

before and after applying the TDEM method. The distribution of the density after the diffusion (Fig. 9) is significantly central at 1, which suggests that the density is effectively equalized.

Besides, it is necessary to check whether the information can be effectively exchanged along the boundaries under our TDEM method. To check it, we will test a certain density distribution on the torus with different boundaries on the planar domain. We consider a ball (Fig. 10) on the torus with the population set to be $2 \cdot \text{Area}(T)$ inside and $\text{Area}(T)$ outside. The torus has radius $(R, r) = (3, 1)$. In this example, we choose three different cut paths and hence get different boundaries on the planar domain. The first choice is that all the cut paths will pass through the center of the ball, while the second choice is that only one of them passes through the center. For the third choice, we consider a set of non-geodesic cut paths. Because of the difference in the cut paths, the density distributions on the corresponding planar domains will be different. Nevertheless, under the TDEM mapping process, the periodicity of the planar domains will be enforced, and hence the three different planar mapping results will give three consistent toroidal density-equalizing maps. Specifically, it can be observed in Fig. 11 that the three TDEM mapping results are nearly identical.

For a more quantitative analysis, in Table 1 we record the statistics of the mapping accuracy and computational efficiency of our TDEM method for all the above-mentioned examples. In particular, we consider the variance of the initial density and the variance of the final density, where both the initial and final densities are normalized so that the average density is 1. This allows us to make a fair comparison between the density variances to assess the density-equalizing effect of the mapping results. It can be observed in all examples that the variance of the final density is significantly smaller than that of the initial density, which suggests that our TDEM method achieves the density-equalizing effect very well.

One may also wonder whether our TDEM method can be applied to toroidal surfaces with different geometries. Here, we consider several tori with different radii and our TDEM method on them. For simplicity, we fix the minor radius as $r = 1$ and vary the major

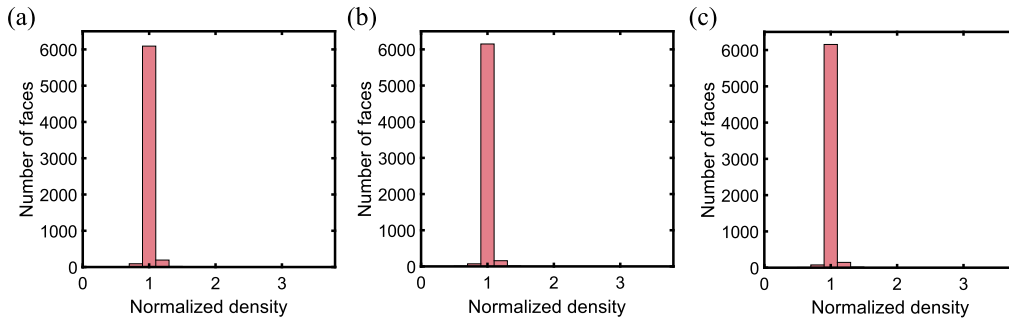


Fig. 11. The normalized final density distributions of the three TDEM mapping results with different cut paths in Fig. 10. (a) The normalized final density for the mapping example in which the cut paths pass through the center of the high-density region. (b) The normalized final density for the mapping example in which only one of the cut paths passes through the center of the high-density region. (c) The normalized final density for the mapping example with non-geodesic cut paths. It can be observed that the three distributions are highly consistent.

Table 1

The performance of our proposed toroidal density-equalizing map (TDEM) method. For each example, we record the variance of the normalized initial density $\text{Var}(\bar{\rho}_{\text{initial}})$ where $\bar{\rho}_{\text{initial}} = \frac{\rho_{\text{initial}}}{\text{mean}(\rho_{\text{initial}})}$, the variance of the normalized final density $\text{Var}(\bar{\rho}_{\text{final}})$ where $\bar{\rho}_{\text{final}} = \frac{\rho_{\text{final}}}{\text{mean}(\rho_{\text{final}})}$, and the time required for the TDEM algorithm.

| Example | $\text{Var}(\bar{\rho}_{\text{initial}})$ | $\text{Var}(\bar{\rho}_{\text{final}})$ | Time (s) |
|------------------|---|---|----------|
| Fig. 1(a) | 0.2552 | 9.8220×10^{-5} | 1.1544 |
| Fig. 5 | 0.1267 | 9.0269×10^{-5} | 0.6034 |
| Fig. 6 | 0.0682 | 9.7357×10^{-5} | 1.3827 |
| Fig. 7 | 0.1642 | 8.5610×10^{-5} | 0.3358 |
| Fig. 8 | 0.6063 | 9.9683×10^{-5} | 3.1409 |
| Fig. 10 (left) | 0.0860 | 9.8329×10^{-5} | 3.0195 |
| Fig. 10 (middle) | 0.0823 | 9.8797×10^{-5} | 2.9125 |
| Fig. 10 (right) | 0.0820 | 9.8667×10^{-5} | 3.0546 |

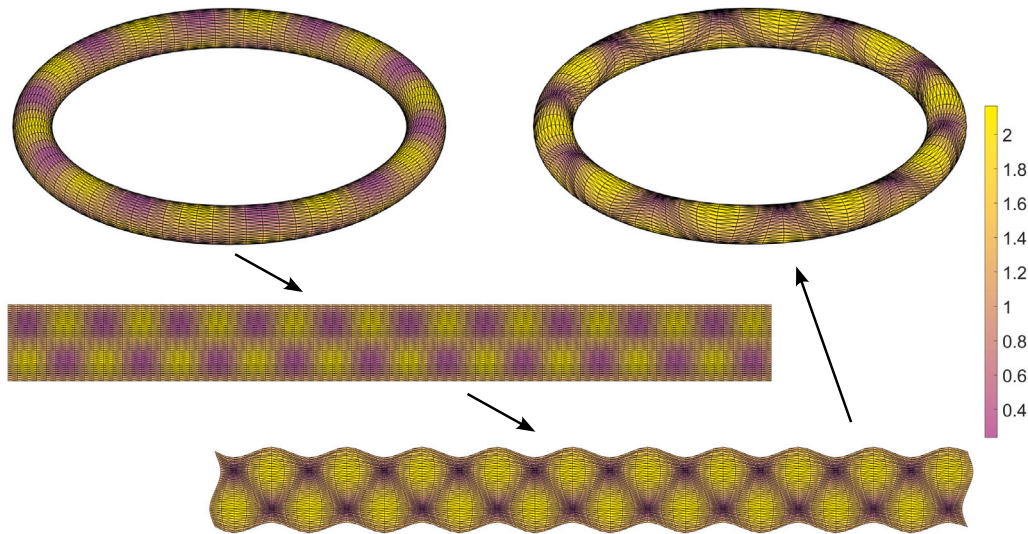


Fig. 12. Mapping a torus with extreme radius parameters $(R, r) = (10, 1)$. The top-left figure panel shows the original toroidal surface with the prescribed population $P(T) = (1.2 - \sin(u)\sin(v))\text{Area}(T)$, where (u, v) is the face centroid of every triangle T under the inverse toroidal projection ϕ^{-1} . The bottom-left panel shows the planar representation of the original toroidal surface under ϕ^{-1} . The bottom-right panel shows the planar mapping result. The top-right panel shows the final TDEM result. All surfaces are color-coded with the initial density $\bar{\rho}_T^{(0)}$.

radius $R = 2, 4, 6, 8, 10$. We then record the performance of our TDEM method on these toroidal surfaces with the input same population $P(T) = (1.2 - \sin(u)\sin(v))\text{Area}(T)$ (see Fig. 12 for the example with $R = 10$). As shown in Table 2, our method can consistently produce accurate toroidal density-equalizing mapping results with the variance of the density significantly reduced. This suggests that our TDEM method is applicable to a wide range of toroidal surfaces with different geometries.

Table 2

The performance of our TDEM method for toroidal surfaces with different geometries. Here, we fix the minor radius $r = 1$ and consider various values of the major radius R . For each example, we record the variance of the normalized initial density $\text{Var}(\bar{\rho}_{\text{initial}})$ where $\bar{\rho}_{\text{initial}} = \frac{\rho_{\text{initial}}}{\text{mean}(\rho_{\text{initial}})}$, the variance of the normalized final density $\text{Var}(\bar{\rho}_{\text{final}})$ where $\bar{\rho}_{\text{final}} = \frac{\rho_{\text{final}}}{\text{mean}(\rho_{\text{final}})}$, and the time required for the TDEM algorithm.

| R | r | $\text{Var}(\bar{\rho}_{\text{initial}})$ | $\text{Var}(\bar{\rho}_{\text{final}})$ | Time (s) |
|-----|-----|---|---|----------|
| 2 | 1 | 0.1654 | 9.8379×10^{-5} | 0.3056 |
| 4 | 1 | 0.1626 | 9.3620×10^{-5} | 0.3194 |
| 6 | 1 | 0.1580 | 9.6483×10^{-5} | 0.3852 |
| 8 | 1 | 0.1519 | 9.8666×10^{-5} | 0.4907 |
| 10 | 1 | 0.1443 | 9.9646×10^{-5} | 0.9653 |

Table 3

The performance of the proposed TDEM method with different time step size δt . Here, the example in Fig. 8 is used. For each δt , we record the variance of the normalized initial density $\text{Var}(\bar{\rho}_{\text{initial}})$ where $\bar{\rho}_{\text{initial}} = \frac{\rho_{\text{initial}}}{\text{mean}(\rho_{\text{initial}})}$, the variance of the normalized final density $\text{Var}(\bar{\rho}_{\text{final}})$ where $\bar{\rho}_{\text{final}} = \frac{\rho_{\text{final}}}{\text{mean}(\rho_{\text{final}})}$, and the time required for the TDEM algorithm.

| δt | $\text{Var}(\bar{\rho}_{\text{initial}})$ | $\text{Var}(\bar{\rho}_{\text{final}})$ | Time (s) |
|------------|---|---|----------|
| 0.05 | 0.6063 | 9.9210×10^{-5} | 6.0471 |
| 0.1 | 0.6063 | 9.9683×10^{-5} | 3.1409 |
| 0.5 | 0.6063 | 9.9849×10^{-5} | 3.0713 |
| 1 | 0.6063 | 9.9552×10^{-5} | 2.9388 |
| 5 | 0.6063 | 9.8105×10^{-5} | 2.5297 |
| 10 | 0.6063 | 9.9519×10^{-5} | 2.2352 |

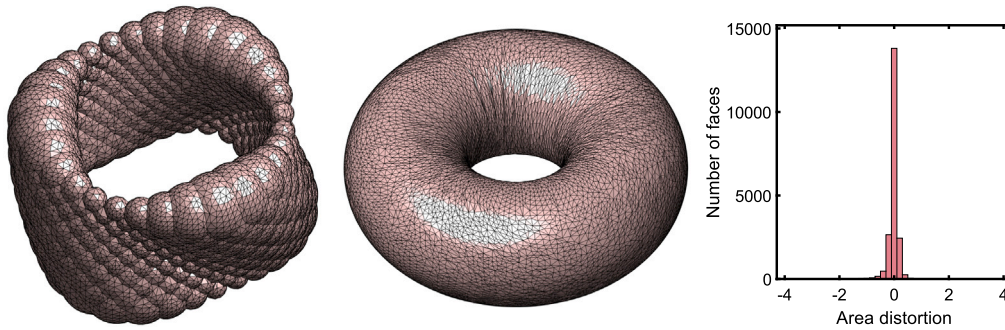


Fig. 13. Toroidal area-preserving parameterization of the Bracelet model. Left to right: The input surface, the parameterization result by our algorithm, and the area distortion histogram.

Another natural question is whether the choice of the time step size δt will largely affect the performance of the proposed TDEM method. To answer this question, here we apply the TDEM algorithm with different choices of time step sizes δt on the example in Fig. 8. The mapping results are summarized in Table 3. Interestingly, it can be observed that the results are almost identical regardless of the choice of δt . This can be explained by the fact that the semi-discrete backward Euler method used for solving the diffusion equation in Eq. (10) is unconditionally stable. Also, while the step size δt would affect the vertex position update in Eq. (14) and potentially lead to mesh overlaps, the subsequent overlap correction and density-deformation recoupling steps can effectively resolve the issue. Altogether, the experiments suggest that we can freely adjust the step size δt without affecting the accuracy.

5.2. Toroidal density-equalizing parameterization

After demonstrating the effectiveness of our proposed TDEM method for computing toroidal density-equalizing maps, we test our proposed toroidal parameterization method for general genus-one surfaces.

Fig. 13 shows an example of computing the toroidal area-preserving parameterization of the genus-one Bracelet surface model from [34]. It can be observed that the original surface geometry is highly complex, with multiple sharp spatial variations in the local area and the surface curvature. Using our proposed method, we can easily parameterize the surface onto a standardized toroidal domain. To assess the area-preserving property of the parameterization, we consider the area distortion d_{area} defined as

$$d_{\text{area}}(f)(T) = \log \left(\frac{(\text{Area}(T))/A}{(\text{Area}(f(T)))/A_f} \right), \quad (17)$$

where $A = \sum_{T' \in \mathcal{F}} \text{Area}(T')$ and $A_f = \sum_{T' \in \mathcal{F}} \text{Area}(f(T'))$. In other words, we study the ratio between the original triangle face area and the triangle face area in the parameterization result after normalizing both the total surface area of the original surface and

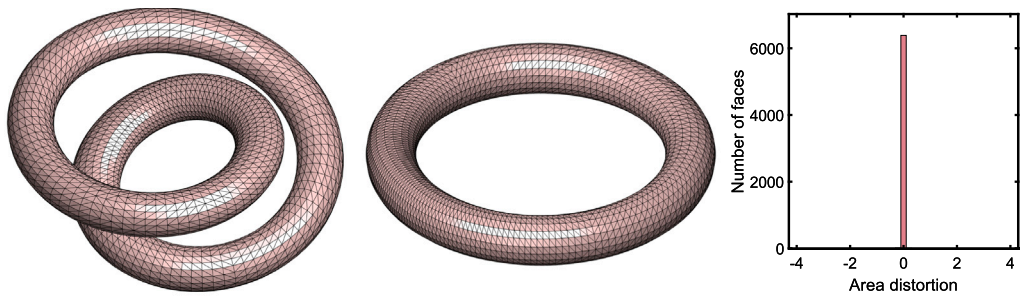


Fig. 14. Toroidal area-preserving parameterization of the Wrapped Tube model. Left to right: The input surface, the parameterization result by our algorithm, and the area distortion histogram.

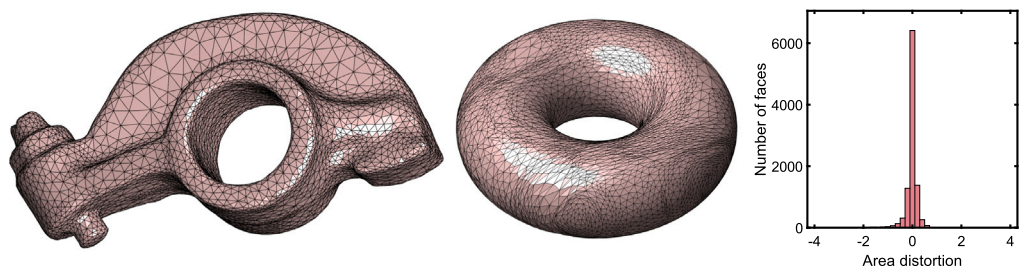


Fig. 15. Toroidal area-preserving parameterization of the Rocker Arm model. Left to right: The input surface, the parameterization result by our algorithm, and the area distortion histogram.

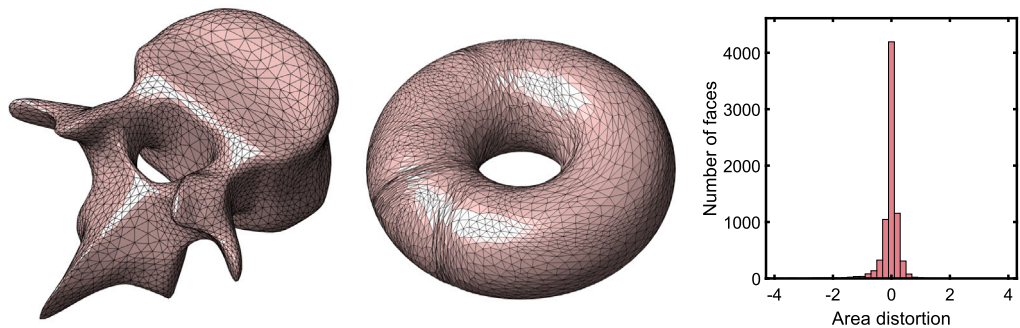


Fig. 16. Toroidal area-preserving parameterization of the Vertebra model. Left to right: The input surface, the parameterization result by our algorithm, and the area distortion histogram.

that of the final torus to be 1. It is easy to see that $d_{\text{area}}(f)(T) = 0$ if and only if $(\text{Area}(T))/A = (\text{Area}(f(T)))/A_f$, i.e., f preserves the normalized face area of the triangle T . As the area distortion histogram in Fig. 13 is highly central at 0, we can see that the toroidal parameterization obtained using our proposed method is highly area-preserving. Fig. 14 shows another genus-one surface model from [35], in which the surface is formed by wrapping an elongated tube and bending it significantly. Using our proposed method, we can easily unwrap the surface and obtain the toroidal area-preserving parameterization. Again, it can be observed from the area distortion histogram that the parameterization is highly area-preserving. In Fig. 15, we further consider parameterizing the genus-one Rocker Arm model. In this example, we can see that the triangle elements in the input surface are highly non-uniform. Nevertheless, using our proposed method, we can effectively obtain a highly area-preserving toroidal parameterization. In Fig. 16, we consider the genus-one Vertebra model. Even for such a model with multiple sharp features, it can be observed that our proposed method can produce a highly area-preserving toroidal parameterization.

In Table 4, we summarize our experimental results and record the area distortion of the initial parameterization h and the final toroidal density-equalizing parameterization f obtained by our proposed method for various surface models. It can be observed that our proposed parameterization method significantly reduces the area distortion of the parameterization by over 85% on average. Altogether, the experimental results show that our proposed toroidal parameterization method is applicable to a wide range of genus-one surfaces.

As shown in the torus example in Figs. 10 and 11 previously, one may consider some arbitrary cut paths while still maintaining high accuracy in the toroidal mapping result. Here, we further study the effect of different cut paths on the genus-1 surface

Table 4

The performance of our proposed toroidal density-equalizing parameterization method. For each example, we set the input population as the triangle face area to achieve a toroidal area-preserving parameterization. For each of the initial parameterization h and final parameterization result f , we record the mean of the absolute value of the area distortion $\text{mean}(|d_{\text{area}}|)$. We also calculate the percentage of improvement in the area distortion to assess the area-preserving performance.

| Example | Mean($ d_{\text{area}}(h) $) | Mean($ d_{\text{area}}(f) $) | % of improvement | Time (s) |
|------------------------|--------------------------------|--------------------------------|------------------|----------|
| Bob (Fig. 1(b)) | 0.7006 | 0.0712 | 89.83% | 4.2759 |
| Bracelet (Fig. 13) | 0.4173 | 0.0987 | 76.35% | 7.1527 |
| Wrapped Tube (Fig. 14) | 0.1865 | 0.0361 | 80.65% | 8.3811 |
| Rocker Arm (Fig. 15) | 1.4689 | 0.1230 | 91.63% | 8.6708 |
| Vertebra (Fig. 16) | 1.5654 | 0.1654 | 89.43% | 12.5335 |

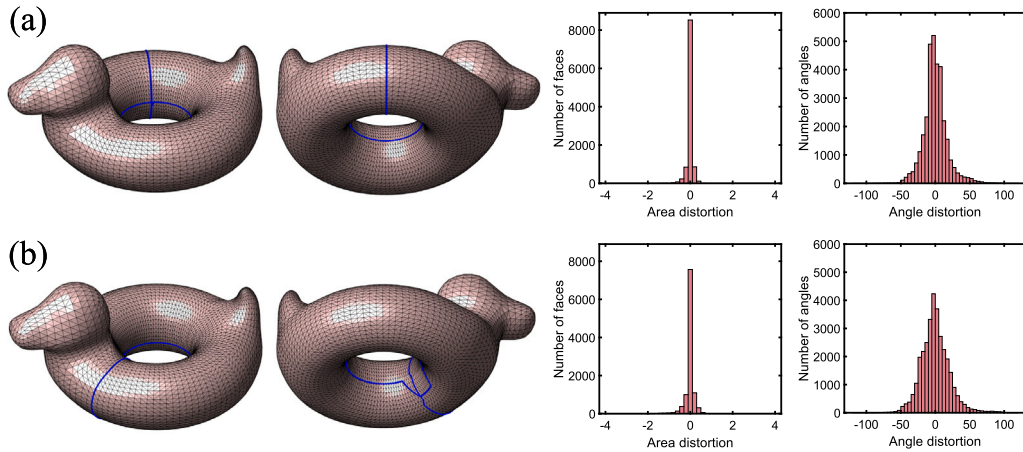


Fig. 17. Comparison between different choices of the cut paths for the toroidal density-equalizing parameterization. (a) The Bob model with a pair of perpendicular geodesic cut paths (with two different views) and the area and angle distortion histograms of the parameterization result. (b) The Bob model with a pair of non-perpendicular and non-geodesic cut paths (with two different views) and the area and angle distortion histograms of the parameterization result.

parameterization results. Specifically, Fig. 17 shows the Bob model with (a) a pair of perpendicular geodesic cut paths and (b) a pair of non-perpendicular and non-geodesic cut paths. We then apply the proposed toroidal density-equalizing parameterization method and assess the area and angle distortion of the results. It can be observed that both choices can lead to highly area-preserving parameterization results, as indicated by the sharp area distortion histograms. Besides the area distortion d_{area} , we also define the angle distortion d_{angle} as the difference between the angles of the triangular faces in the mapping results and those in the input surface model. By comparing the peaks of the area and angle distortion histograms obtained from the two choices of cut paths, we can see that the choice of the perpendicular geodesic cut paths yields a better result in terms of both the area and angle distortions. Therefore, in general, it is recommended to utilize perpendicular geodesic cut paths.

Besides, in previous examples, the radii R and r of the mapped torus are prescribed by the user. One may ask whether it is possible to determine some suitable values of R and r automatically based on certain criteria. Here, we propose a method to determine (R, r) using certain key geometric features of the input surface S . Since it is natural to construct a torus that matches the overall shape of the input genus-one surface S as much as possible, here we consider setting the radius r by utilizing the lengths l_1, l_2 of the cut paths. Specifically, it is desired that the perimeter of the small circle matches the length of the shorter cut path. This gives

$$2\pi r = \min\{l_1, l_2\} \iff r = \frac{\min\{l_1, l_2\}}{2\pi}.$$

Also, it is natural to consider that the surface area of the torus matches that of the input surface. Therefore, we can further set R using:

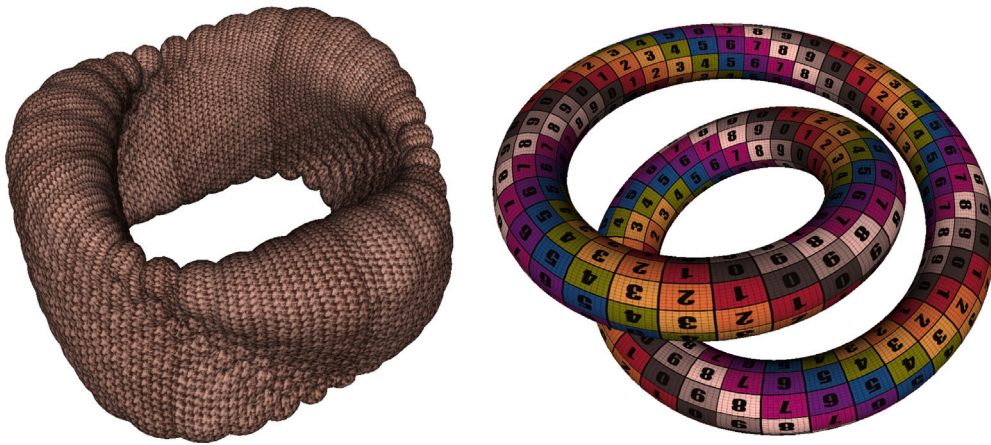
$$4\pi^2 Rr = \text{Area}(S) \iff R = \frac{\text{Area}(S)}{4\pi^2 r}.$$

In Table 5, we consider mapping the Bracelet model in Fig. 13 onto toroidal surfaces with different radii R, r . We first consider some arbitrary choices of (R, r) as in Table 2. Then, we also consider using the length, width and height of the Bracelet model to set the radii, yielding $(R, r) = (6.4751, 3.9755)$. Finally, we use our above-mentioned criterion to determine the radii based on the geometric features of the input surface, which gives $(R, r) = (5.5013, 2.5582)$. By comparing the area and angle distortions of the mapping results, we can see that the proposed method gives both the lowest area distortion and the lowest angle distortion. This demonstrates the effectiveness of using the geometric features of the input surface for determining suitable radii of the target toroidal surface.

Table 5

Comparison between different choices of the radii (R, r) of the target toroidal surface for mapping the Bracelet model. Here, we first consider some arbitrary choices of (R, r) as in Table 2. Then, we also consider determining (R, r) using the length, width and height of the Bracelet model, which gives $(R, r) = (6.4751, 3.9755)$. Finally, we consider our proposed geometry-based criterion for setting (R, r) , which gives $(5.5013, 2.5582)$. It can be observed that our proposed criterion gives the best result in terms of both the area distortion d_{area} and the angle distortion d_{angle} .

| R | r | R/r | Mean($ d_{\text{area}} $) | Std(d_{area}) | Mean($ d_{\text{angle}} $) | Std(d_{angle}) |
|--------|--------|--------|-----------------------------|--------------------------|------------------------------|---------------------------|
| 2 | 1 | 2 | 0.0901 | 0.1597 | 18.6540 | 23.4004 |
| 4 | 1 | 4 | 0.0905 | 0.1887 | 20.5323 | 25.9060 |
| 6 | 1 | 6 | 0.1158 | 0.2605 | 28.5585 | 34.4406 |
| 6.4751 | 3.9755 | 1.6287 | 0.1072 | 0.1847 | 19.8793 | 25.9751 |
| 5.5013 | 2.5582 | 2.1505 | 0.0889 | 0.1565 | 18.2916 | 22.6589 |

**Fig. 18.** Texture mapping of genus-one surfaces using our proposed toroidal parameterization method.

Using the proposed toroidal density-equalizing parameterization method, we can effectively perform seamless texture mapping for genus-one surfaces. Specifically, to design a texture on a given genus-one surface, we can map it onto a prescribed toroidal domain using the proposed parameterization method. Next, we can easily create texture patterns on the toroidal surface or its associated planar domain under the inverse toroidal projection ϕ^{-1} . Finally, we can map the designed texture back to the given surface using the inverse of the toroidal parameterization. To illustrate this idea, in Fig. 18 we show genus-one surface texture mapping examples obtained using the above-mentioned approach. Because of the density-equalizing property of the proposed parameterization method, we can easily control the area change in different regions, thereby controlling the uniformity of the texture on the given surface. From the texture mapping examples, it can be observed that the textures are highly uniform. This shows that our method is well-suited for genus-one surface texture mapping.

6. Conclusion and discussion

In this paper, we have developed a novel method for computing density-equalizing maps for toroidal surfaces. We have shown that a large variety of toroidal shape deformation effects can be achieved by prescribing different population functions for the density diffusion process. We have also developed a toroidal density-equalizing parameterization method for general genus-one surfaces, which allows us to easily achieve toroidal parameterizations with controllable area changes. In particular, we have demonstrated the effectiveness of our method for computing toroidal area-preserving parameterizations.

As we have shown in our experiments, our proposed TDEM method can be flexibly applied to toroidal surfaces with different major and minor radii. Therefore, a natural next step is to extend the proposed toroidal parameterization method by incorporating an optimization procedure to further optimize the toroidal geometry and reduce not only the density-equalizing errors but also other geometric distortions of the parameterization results. Another possible future direction is to utilize the proposed methods for the shape analysis of genus-one surfaces.

Besides, note that in the proposed method, the analytical parameterization of the torus ϕ is only used for building a correspondence between the planar domain and the toroidal surface, which allows us to perform the computation of the planar domain while taking the difference between the planar domain and the torus into consideration. Therefore, in case it is desirable to compute mappings onto other prescribed surfaces without any analytical parameterization, one may simply replace ϕ with other discrete interpolations, which would then allow us to obtain the final mapping result after performing the planar computation.

Acknowledgments

This work was supported in part by the National Natural Science Foundation of China Young Scientists Fund, Project Code 12401503 (to G. P. T. Choi).

Data availability

The code and data are available on GitHub at <https://github.com/garyptchoi/toroidal-density-equalizing-map>.

References

- [1] M.T. Gastner, M.E.J. Newman, Diffusion-based method for producing density-equalizing maps, *Proc. Natl. Acad. Sci.* 101 (20) (2004) 7499–7504.
- [2] V. Colizza, A. Barrat, M. Barthélemy, A. Vespignani, The role of the airline transportation network in the prediction and predictability of global epidemics, *Proc. Natl. Acad. Sci.* 103 (7) (2006) 2015–2020.
- [3] D.B. Wake, V.T. Vredenburg, Are we in the midst of the sixth mass extinction? A view from the world of amphibians, *Proc. Natl. Acad. Sci.* 105 (supplement_1) (2008) 11466–11473.
- [4] J. Lenoir, R. Bertrand, L. Comte, L. Bourgeaud, T. Hattab, J. Muriene, G. Grenouillet, Species better track climate warming in the oceans than on land, *Nat. Ecol. Evol.* 4 (8) (2020) 1044–1059.
- [5] K.S. Gleditsch, M.D. Ward, Diffusion and the international context of democratization, *Int. Organ.* 60 (4) (2006) 911–933.
- [6] A. Mislove, S. Lehmann, Y.-Y. Ahn, J.-P. Onnela, J. Rosenquist, Understanding the demographics of Twitter users, *Proc. Int. AAAI Conf. Web Soc. Media* 5 (1) (2011) 554–557.
- [7] M.T. Gastner, V. Seguy, P. More, Fast flow-based algorithm for creating density-equalizing map projections, *Proc. Natl. Acad. Sci.* 115 (10) (2018) E2156–E2164.
- [8] I.K. Duncan, S. Tingsheng, S.T. Perrault, M.T. Gastner, Task-based effectiveness of interactive contiguous area cartograms, *IEEE Trans. Vis. Comput. Graphics* 27 (3) (2020) 2136–2152.
- [9] K.L. Fung, S.T. Perrault, M.T. Gastner, Effectiveness of area-to-value legends and grid lines in contiguous area cartograms, *IEEE Trans. Vis. Comput. Graphics* 30 (8) (2024) 4631–4647.
- [10] G.P.T. Choi, C.H. Rycroft, Density-equalizing maps for simply connected open surfaces, *SIAM J. Imaging Sci.* 11 (2) (2018) 1134–1178.
- [11] Z. Lyu, G.P.T. Choi, L.M. Lui, Bijective density-equalizing quasiconformal map for multiply connected open surfaces, *SIAM J. Imaging Sci.* 17 (1) (2024) 706–755.
- [12] Z. Li, S. Aryana, Diffusion-based cartogram on spheres, *Cartogr. Geogr. Inf. Sci.* 45 (5) (2018) 464–475.
- [13] Z. Lyu, L.M. Lui, G.P.T. Choi, Spherical density-equalizing map for genus-0 closed surfaces, *SIAM J. Imaging Sci.* 17 (4) (2024) 2110–2141.
- [14] Z. Lyu, L.M. Lui, G.P.T. Choi, Ellipsoidal density-equalizing map for genus-0 closed surfaces, 2024, arXiv preprint arXiv:2410.12331.
- [15] Z. Li, S.A. Aryana, Visualization of subsurface data using three-dimensional cartograms, in: *Advances in Remote Sensing and Geo Informatics Applications: Proceedings of the 1st Springer Conference of the Arabian Journal of Geosciences (CAJG-1)*, Tunisia 2018, Springer, 2019, pp. 17–19.
- [16] G.P.T. Choi, C.H. Rycroft, Volumetric density-equalizing reference map with applications, *J. Sci. Comput.* 86 (3) (2021) 41.
- [17] G.P.T. Choi, B. Chiu, C.H. Rycroft, Area-preserving mapping of 3D carotid ultrasound images using density-equalizing reference map, *IEEE Trans. Biomed. Eng.* 67 (9) (2020) 2507–2517.
- [18] M. Shaqfa, G.P.T. Choi, G. Anciaux, K. Beyer, Disk harmonics for analysing curved and flat self-affine rough surfaces and the topological reconstruction of open surfaces, *J. Comput. Phys.* 522 (2025) 113578.
- [19] G.P.T. Choi, M. Shaqfa, Hemispheroidal parameterization and harmonic decomposition of simply connected open surfaces, *J. Comput. Appl. Math.* 461 (2025) 116455.
- [20] M.S. Floater, K. Hormann, Surface parameterization: a tutorial and survey, in: *Advances in Multiresolution for Geometric Modelling*, Springer, 2005, pp. 157–186.
- [21] A. Sheffer, E. Praun, K. Rose, Mesh parameterization methods and their applications, *Found. Trends Comput. Graph. Vis.* 2 (2) (2007) 105–171.
- [22] D. Steiner, A. Fischer, Planar parameterization for closed 2-manifold genus-1 meshes, in: *Proceedings of the Ninth ACM Symposium on Solid Modeling and Applications*, 2004, pp. 83–91.
- [23] N. Ray, W.C. Li, B. Lévy, A. Sheffer, P. Alliez, Periodic global parameterization, *ACM Trans. Graph.* 25 (4) (2006) 1460–1485.
- [24] W. Zeng, X. Li, S.-T. Yau, X. Gu, Conformal spherical parametrization for high genus surfaces, *Commun. Inf. Syst.* 7 (3) (2007) 273–286.
- [25] K.C. Lam, X. Gu, L.M. Lui, Landmark constrained genus-one surface Teichmüller map applied to surface registration in medical imaging, *Med. Image Anal.* 25 (1) (2015) 45–55.
- [26] M.-H. Yueh, T. Li, W.-W. Lin, S.-T. Yau, A new efficient algorithm for volume-preserving parameterizations of genus-one 3-manifolds, *SIAM J. Imaging Sci.* 13 (3) (2020) 1536–1564.
- [27] U. Pinkall, K. Polthier, Computing discrete minimal surfaces and their conjugates, *Exp. Math.* 2 (1) (1993) 15–36.
- [28] T.W. Meng, G.P.-T. Choi, L.M. Lui, TEMPO: Feature-endowed Teichmüller extremal mappings of point clouds, *SIAM J. Imaging Sci.* 9 (4) (2016) 1922–1962.
- [29] G.P.T. Choi, Efficient conformal parameterization of multiply-connected surfaces using quasi-conformal theory, *J. Sci. Comput.* 87 (3) (2021) 70.
- [30] A. Jacobson, Common 3D test models, 2023, <https://github.com/alecjacobson/common-3d-test-models>. (Accessed 07 October 2024).
- [31] Q. Zhou, A. Jacobson, Thingi10k, 2017, <https://ten-thousand-models.appspot.com/>. (Accessed 17 October 2024).
- [32] K. Crane, Keenan's 3D model repository, 2014, <http://www.cs.cmu.edu/~kmc Crane/Projects/ModelRepository/>. (Accessed 07 October 2024).
- [33] H. Edelsbrunner, 180 wrapped tubes, 2001, <https://pub.ista.ac.at/~edels/Tubes/>. (Accessed 07 October 2024).
- [34] Q. Zhou, A. Jacobson, Thingi10k: A dataset of 10,000 3D-printing models, 2016, arXiv preprint arXiv:1605.04797.
- [35] H. Edelsbrunner, 180 wrapped tubes, *J. Univers. Comput. Sci.* 7 (5) (2001) 379–399.